ChemPubSoc Europe

DOI: 10.1002/chem.201403551

CHEMISTRY
A European Journal
Communication

Drug Delivery

Drug Encapsulation and Release by Mesoporous Silica Nanoparticles: The Effect of Surface Functional Groups

Si Yu Tan,[a] Chung Yen Ang,[a] Peizhou Li,[a] Qi Ming Yap,[a] and Yanli Zhao*[a, b]

Abstract: Mesoporous silica nanoparticles (MSNPs) have been widely used as drug carriers for stimuli-responsive drug delivery. Herein, a catalysis screening technique was adopted for analyzing the effects of chain length, terminal group, and density of disulfide-appended functional ligands on the surface of MSNPs on drug-loading capacity and glutathione-triggered drug-release kinetics. The ligand with an intermediate length (5 carbon atoms) and a bulky terminal group (cyclohexyl) that complexes with theβ-cyclodextrin ring showed the highest drug loading capacity as well as good release kinetics. In addition, decreasing the surface coverage of the functional ligands led to an enhancement in drug release. In vitro drug-delivery experiments on a melanoma cell line (B16-F10) by using the functionalized MSNPs further supported the conclusion. The results obtained may serve as a general guide for developing more effective MSNP systems for drug delivery.

Mesoporous silica nanoparticles (MSNPs) have shown various potential biomedical applications, particularly as nanocarriers for drug delivery.[1] Their ease of synthesis and tunable properties make MSNPs highly customizable according to desired purpose.[2] Furthermore, its high surface area allows the grafting of a large number of functional groups on the surface so as to impart various interesting properties to MSNPs.[3] One of the properties that can be imparted onto MSNPs is stimulated release of loaded cargos through the grafting of capping groups. Stimulated cargo release has been widely utilized as a key strategy for the specific release of drugs in a controlled manner[4] in order to reduce side effects brought about by the use of anticancer drugs for chemotherapy. One common stimulation method is redox activation based on glutathione (GSH) in cancer cells,[5] as it has been shown that some cancer cells express a significant amount of intracellular GSH compared to healthy cells.[6] Under this strategy, the surface of MSNPs are bridged with capping agents through a disulfide linkage.[7] In this way, intracellular GSH would induce reductive cleavage of the disulfide bond, thereby removing the capping agents and releasing the loaded drugs. In a study by Zink and co-workers,[8] the effect of complexation of α-cyclodextrin (α-CD) with aniline units on hollow MSNPs on drug release was investigated. Amorós and co-workers, on the other hand, investigated the relationship between different alkyl chain lengths and drug release behavior.[9] In a recent work by Gaberšček and co-workers, redox-responsive systems with different level of hindrance on the disulfide linkage were studied, showing that an increase in hindrance results in slower release.[10] Although some studies based on GSH-triggered drug release in vitro and in vivo have been reported,[11] the effect of terminal group, chain length, and amount of disulfide unit on the MSNP surface on drug loading and release is still not well understood.

Herein, we report a catalysis screening method to study the effect of chain length, terminal group, and disulfide amount on the surface of MSNPs on drug-loading capacity and release kinetics (Figure 1). Supramolecular complexes involving β-cyclodextrin (β-CD) and the terminal groups of different functional ligands were employed in this study owing to the ease of functionalizing the surface of MSNPs. A systemic approach was adopted, whereby ligands with different chain lengths were first tested. Thereafter, the chain length that gave the highest release capability was used for the following tests that involved different types of terminal units. Then, the effect of varying the amount of disulfide unit on the surface was investigated by using the functional ligand that showed the highest release ability. Finally, in vitro drug-delivery experiments were conducted on a melanoma cell line (B16-F10) by using the functionalized MSNPs screened. We here selected doxorubicin (DOX) as the cargo within MSNPs, as DOX is a common anticancer drug that is loaded into MSNPs for drug-delivery applications.

We begin the studies by first synthesizing MCM-41 MSNPs by using a surfactant-directed technique with hexadecyltrimethylammonium bromide (CTAB) as the surfactant. The as-synthesized MSNPs were characterized by transmission electron microscopy (TEM), and the results showed that the obtained MSNPs were spherical in shape with diameter of 70–80 nm. The Brunauer–Emmett–Teller (BET) measurements showed a type IV adsorption/desorption isotherm, which is a characteristic feature of mesoporous materials. The BET measurements also show that the MSNPs possessed a high BET surface area of 921 $m^2 g^{-1}$ with a Barrett–Joyner–Halenda (BJH) pore size of 3.03 nm, which is slightly larger than the pore size (3.56 nm) measured using powder X-ray diffraction (XRD). These characterizations confirmed the successful synthesis of the MSNPs. After grafting the surface with a mercaptan group, X-ray photoelectron spectroscopic (XPS) analysis of mercaptan-grafted MSNPs, that is, **MSNPs-3(1)**, shows the presence of an S 2p peak at 163.6 eV, indicating successful conjugation of the mercaptan group onto the surface. The FT-IR spectrum presents clear alkyl C–H peaks, corresponding to the propyl groups of the grafted 3-mercaptopropyltrimethoxysilane.

The next step was the synthesis of a series of thiol-activated ligands (Figure 2) for conjugating with the mercaptan-grafted MSNPs. Thus, the conjugation of the *n*-bromo-terminated carboxylic acids of different chain lengths with a variety of alkyl (R) amines was carried out, followed by the conversion of the bromide groups into the thiol groups. The obtained ligands were then coupled onto the surface of MSNPs prior to DOX

[a] *S. Y. Tan,[+] C. Y. Ang,[+] P. Li, Q. M. Yap, Prof. Dr. Y. Zhao*
Division of Chemistry and Biological Chemistry
School of Physical and Mathematical Sciences
Nanyang Technological University
21 Nanyang Link, Singapore 637371 (Singapore)
E-mail: zhaoyanli@ntu.edu.sg
Homepage: http://www.ntu.edu.sg/home/zhaoyanli/

[b] *Prof. Dr. Y. Zhao*
School of Materials Science and Engineering
Nanyang Technological University
Singapore 639798 (Singapore)

[+] *These authors contributed equally to this work.*

Supporting information for this article is available on the WWW under http://dx.doi.org/10.1002/chem.201403551.

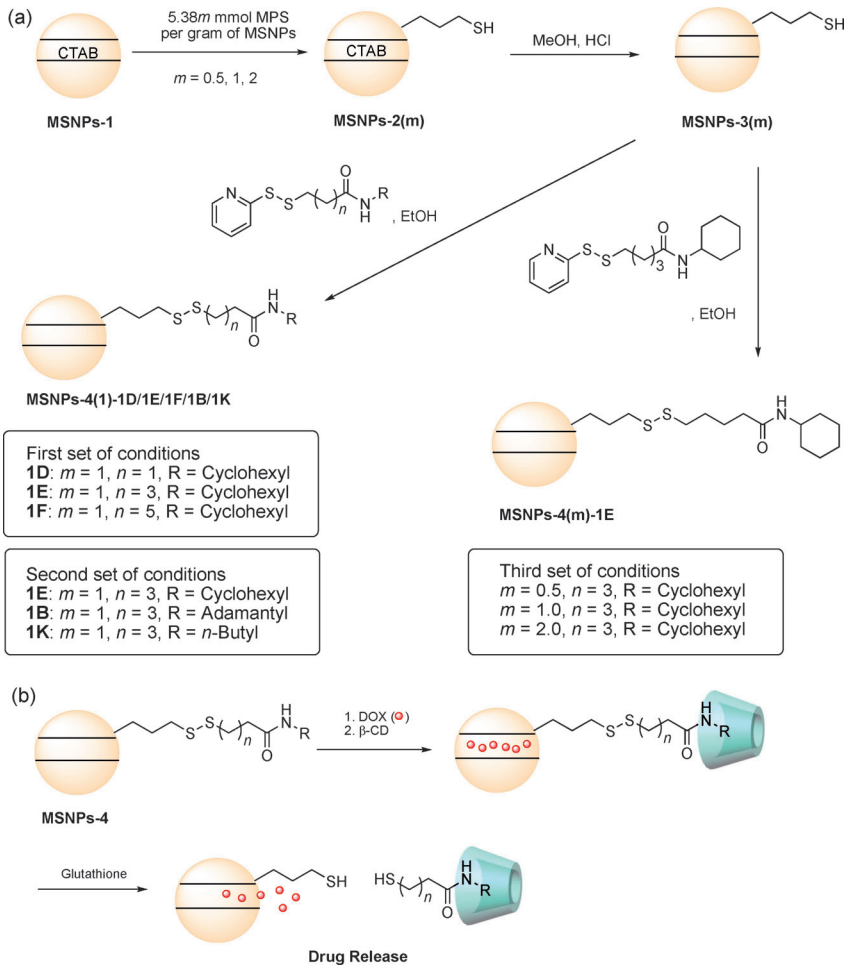

Figure 1. a) Synthesis of different types of functional MSNPs under different conditions. First set of conditions screened involved the use of ligands with different chain lengths. The second set of conditions tested was the effect of the terminal groups with different sizes. Lastly, different amounts of the same ligand were conjugated onto the surface of MSNPs to investigate the effects towards the surface coverage, drug loading capacity and release kinetics. *m* indicates the volume (mL) of 3-mercaptopropyltrimethoxysilane (MPS) used per 1 g of MSNPs. b) Synthetic representation for the release mechanism from β-CD-capped and DOX-loaded MSNPs triggered by GSH.

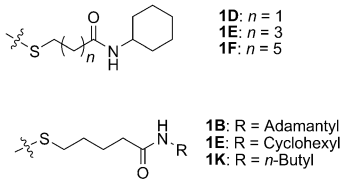

Figure 2. Ligands conjugated onto the surface of MSNPs for investigating the effect of ligand length and bulkiness.

loading and complexed with β-CD. The complexation of β-CD with these (R) ending groups could keep the loaded drug within the mesopores without leakage. Thereafter, the DOX loading capacity and release profiles of functionalized MSNPs were measured accordingly.

The first set of conditions tested was the effect of ligand length on the drug-capping and release efficiency. Ligands with varying lengths (3, 5, and 7 carbon atoms) and cyclohexyl terminal group were used. After conjugation of the respective ligands onto the surface of MSNPs, XPS was adopted to measure the amount of functional ligands on the surface of MSNPs, that is, **MSNPs-4(1)-1D**, **MSNPs-4(1)-1E**, and **MSNPs-4(1)-1F**. The results (Table 1) show that the sulfur content of **MSNPs-3(1)**, **MSNPs-4(1)-1D**, **MSNPs-4(1)-1E** are similar, ca. 12.6–14.9%. However, **MSNPs-4(1)-1F** showed a slightly higher sulfur content (ca. 15.3%) upon conjugation of ligand **1F** to the surface of **MSNPs-3(1)**. As ligand **1F** is longer and thus having a lower steric effect, more ligand would conjugate onto the surface of **MSNPs-3(1)**.

Thus, the **MSNPs-4(1)** series was employed for evaluating drug-loading capacity. Table 1 summarizes the DOX loading capacity of these functionalized MSNPs. The order of DOX loading capacity was **MSNPs-4(1)-1E** > **MSNPs-4(1)-1F** > **MSNPs-4(1)-1D**. This observation was surprising as we initially expected that **MSNPs-4(1)-1F** would have the highest drug-loading capacity owing to it having the largest number of ligands functionalized on the surface of MSNPs. The results, however, showed that ligand **1E**, having 5 carbon atoms, gave the highest DOX loading capacity, 13.9%. The reason for such a high loading capacity may be that ligand **1E** possesses the ideal length for the drug to enter into the mesopores and the ability to retain the drug within the mesopores after capping with β-CD. **MSNPs-4(1)-1F** exhibited a loading capacity of 13.2%. After capping ligand **1F** with β-CD, β-CD is a bit far away from the surface of MSNPs, thus not being able to efficiently block the mesopores for drug storage. The slight leakage of the loaded drug during the washing process may in turn explain the lower drug-loading capability of **MSNPs-4(1)-1F** compared with **MSNPs-4(1)-1E**. Although **MSNPs-4(1)-1D** has approximately the same amount of ligands on the surface as **MSNPs-4(1)-1E**, the cyclohexyl group is much closer to the mesopores of MSNPs. This makes the drug-loading process difficult and thus results in a low drug-loading capacity compared with **MSNPs-4(1)-1E**.

Then, the release profiles were obtained to investigate the effect of chain length. Figure 3 shows that **MSNPs-4(1)-1E**

Table 1. XPS data indicating the sulfur content after the conjugation of respective ligands with different chain lengths on the surface of MSNPs. In addition, the DOX loading capacity with standard deviation was obtained for **MSNPs-4(1)-1D**, **MSNPs-4(1)-1E**, and **MSNPs-4(1)-1F**.

MSNPs	% Si	% S[a]	Loading capacity
MSNPs-3(1)	87.4	12.6	–
MSNPs-4(1)-1D	85.1	14.9	12.2 ± 0.8
MSNPs-4(1)-1E	85.3	14.7	13.9 ± 0.3
MSNPs-4(1)-1F	84.6	15.4	13.2 ± 0.9

[a] The sulfur content corresponds to the amount of ligands being conjugated onto the surface of MSNPs.

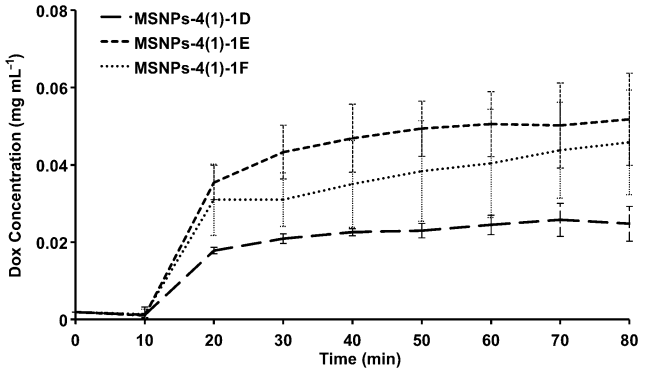

Figure 3. DOX release kinetics for **MSNPs-4(1)-1D**, **MSNPs-4(1)-1E**, and **MSNPs-4(1)-1F** when GSH (10 mM) was added at the 10th minute.

gave the highest release followed by **MSNPs-4-1F** and lastly **MSNPs-4(1)-1D**. These results are consistent with the DOX loading capacity, indicating that the interaction of GSH with the disulfide bond on the MSNP surface leads to the uncapping of the β-CD complexes for drug release. The complexation of β-CD did not have an obvious influence on the cleavage of the disulfide bond. Because **MSNPs-4(1)-1E** showed the highest level of release, this system was chosen for the next set of experiments.

After the effect of chain length was investigated, we varied the terminal groups for complexation with β-CD. As the cyclohexyl end group was used in ligand **1E**, two other end groups, adamantyl and *n*-butyl, were selected for comparison studies. The adamantyl end group serves as a more bulky counterpart of the cyclohexyl group, while the *n*-butyl group only consists of 4 carbon atoms. To investigate the effect of these terminal groups on the DOX loading capacities and release profiles, their binding constants involving complexation with β-CD were determined. Table 2 shows the average binding constants obtained from the Hildebrand plot of ^{1}H NMR chemical shifts of the different terminal groups with β-CD. As expected, the adamantyl group gave the highest binding constant with β-CD, followed by the cyclohexyl group. Because the R^2 value of the binding constant between *n*-butylamine and β-CD was very large, the binding constant was considered to be very low.

After obtaining the different binding constants, the conjugation of the different ligands (1B, 1E, 1K) onto the surface of

Table 2. Binding constants for the different terminal groups with β-CD.

Terminal group	Binding constant calculated from region 1 (R^2 value)	Binding constant calculated from region 2 (R^2 value)	Average
adamantamine	2044 (0.9725)	3072 (0.9981)	2873
cyclohexylamine	265 (0.9973)	322 (0.9727)	293
n-butylamine	1545 (0.7989)	1766 (0.7339)	–[a]

[a] Binding constant of *n*-butylamine with β-CD was also determined. Since the R^2 value was very big, the binding constant was considered to be very low.

MSNPs was studied using XPS. The XPS data of functionalized MSNPs show different sulfur contents, thus representing different amounts of ligands on the surface of functionalized MSNPs. **MSNPs-4(1)-1K** exhibits the highest sulfur content followed by **MSNPs-4(1)-1B** and lastly **MSNPs-4(1)-1E**. This order is due to the differences in the flexibility and size of the end groups. The small and flexible *n*-butyl group facilitates the conjugation of ligand **1K** to the MSNP surface, resulting in the highest sulfur content. The adamantyl and cyclohexyl groups, on the other hand, are much larger than the *n*-butyl group, thus leading to a low density of functional groups on the surface. The rigid adamantyl group may be able to arrange more neatly on the surface of MSNPs as compared with the cyclohexyl group, leading to conjugation of more ligand **1B** on the surface than ligand **1E**. Thus, the structural nature of these ligands could be used to explain the results obtained in Table 3.

Table 3. XPS data indicating the sulfur content upon conjugation of different ligands on the surface of MSNPs. In addition, the DOX loading capacity was obtained for **MSNPs-4(1)-1B**, **MSNPs-4(1)-1E**, and **MSNPs-4(1)-1K**.

MSNPs	% Si	% S[a]	Loading capacity
MSNPs-3(1)	87.4	12.6	–
MSNPs-4(1)-1B	85.4	15.6	11.7 ± 0.2
MSNPs-4(1)-1E	85.3	14.7	13.9 ± 0.3
MSNPs-4(1)-1K	83.1	16.9	13.1 ± 0.1

[a] The sulfur content corresponds to the amount of ligands being conjugated onto the surface of MSNPs.

The order of loading capacity for this series of functionalized MSNPs was **MSNPs-4(1)-1E** > **MSNPs-4(1)-1K** > **MSNPs-4(1)-1B** (Table 3). The loading capacity was mainly dependent on two factors: firstly, the amount of the ligand on the surface of MSNPs in relation to access to the mesopores, and secondly, the binding of the ligand with β-CD to prevent the loaded drug from escaping. **MSNPs-4(1)-1B** gave the lowest loading capacity, although XPS showed that there was a substantial amount of the ligand on the surface of MSNPs. The low level of loading capacity might be due to the steric effect of the adamantyl group, which prevents the drug from entering the mesopores of MSNPs during the loading process. Compared with **MSNPs-4(1)-1K** with the *n*-butyl end group, **MSNPs-4(1)-1E** showed higher loading capacity on account of the higher

binding constant of the cyclohexyl end group with β-CD to better keep the loaded drug within the mesopores. The DOX release behavior of these systems was then tested, indicating that the trend of the release profiles matches the trend of the DOX loading capacities (Figure 4). The observation further supports that the interaction of GSH with the disulfide bond was consistent for all the functionalized MSNPs. By comparing the release profiles for this set of conditions, **MSNPs-4(1)-1E** again gave the highest level of release and was chosen for the last set of experiments.

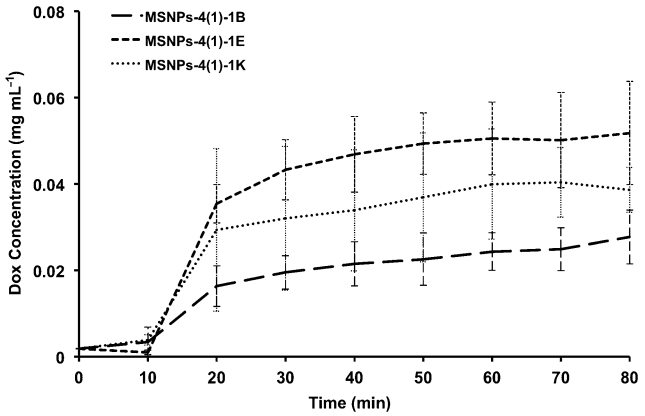

Figure 4. Release kinetics for **MSNPs-4(1)-1B**, **MSNPs-4(1)-1E**, and **MSNPs-4(1)-1K** when GSH (10 mM) was added at the 10th minute.

The last set of conditions to be explored would be the effect of different amount of the ligands on the surface towards the DOX loading capacity and release efficiency. Firstly, XPS was again used to quantify the amount of thiol units as well as the final ligand on the surface of MSNPs. From the XPS data in Table 4, an increase in the sulfur content was observed when more mercaptan groups were grafted on the surface, giving the following order in terms of the sulfur content: **MSNPs-3(2)** > **MSNPs-3(1)** > **MSNPs-3(0.5)**. After conjugation of the final ligands onto the surface through disulfide bond formation, the same order in sulfur content was observed: **MSNPs-4(2)-1E** > **MSNPs-4(1)-1E** > **MSNPs-4(0.5)-1E**. The increase in sulfur content after conjugation was proportional to the type of MSNPs, making the comparison of the drug-loading capacity easier.

Table 4. XPS data indicating the sulfur content after grafting different amount of mercaptan groups on the surface of MSNPs as well as after further conjugation of different amount of ligand **1E** on the surface. In addition, the DOX loading capacity was obtained for **MSNPs-4(0.5)-1E**, **MSNPs-4(1)-1E**, and **MSNPs-4(2)-1E**.

MSNPs	% Si	% S[a]	Loading capacity
MSNPs-3(0.5)	88.1	11.9	–
MSNPs-4(0.5)-1E	86.9	13.1	11.2 ± 0.1
MSNPs-3(1)	87.4	12.6	–
MSNPs-4(1)-1E	85.3	14.7	13.9 ± 0.2
MSNPs-3(2)	85.6	14.4	–
MSNPs-4(2)-1E	82.7	17.3	11.3 ± 0.7

[a] The sulfur content corresponds to the amount of ligands being conjugated onto the surface of MSNPs.

The loading capacity of various functionalized MSNPs is presented in Table 4, and the results reveal that the loading capacity of **MSNPs-4(1)-1E** is higher than that of **MSNPs-4(2)-1E** and **MSNPs-4(0.5)-1E**. Although **MSNPs-4(2)-1E** showed the highest amount of ligands on the surface of MSNPs, its loading capacity was lower, as the excessive amount of cyclohexyl groups on the surface could block the mesopores for drug loading. **MSNPs-4(0.5)-1E** also gave a low loading capacity because having less ligands on the surface cannot well retain a large amount of DOX within the mesopores. Thus, **MSNPs-4(1)-1E** has a reasonable amount of ligands on the surface to allow sufficient loading of DOX into the mesopores without obvious leakage. The level of drug release of these different samples gave the following trend: **MSNPs-4(0.5)-1E** > **MSNPs-4(1)-1E** > **MSNPs-4(2)-1E** (Figure 5). This order was unexpected

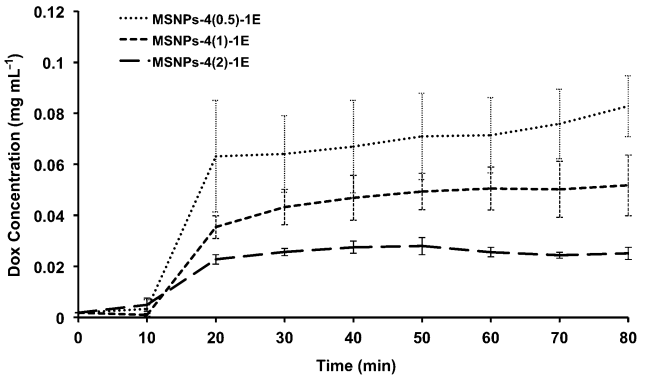

Figure 5. Release kinetics for **MSNPs-4(0.5)-1E**, **MSNPs-4(1)-1E**, and **MSNPs-4(2)-1E** when GSH (10 mM) was added at the 10th minute.

because the loading capacity was proportional to the release profile in above two sets of conditions tested. In this experiment, although **MSNPs-4(0.5)-1E** did not give the highest loading capacity, the amount of DOX released from **MSNPs-4(0.5)-1E** was the most significant. This is probably because the low amount of ligands on the surface enables GSH to easily interact with the disulfide bond, thus removing the capping agents for drug release. This explanation could be supported by the release profile of **MSNPs-4(2)-1E**, where the lowest amount of release was observed. The surface of **MSNPs-4(2)-1E** is highly hindered owing to the presence of a large amount of ligands capped with β-CD, thus preventing GSH from reacting with the disulfide bond.

To investigate the applicability of these functional MSNPs, in vitro drug-delivery experiments were carried out on the B16-F10 melanoma cell line. B16-F10 cells were incubated with **MSNPs-4(0.5)-1E**, **MSNPs-4(1)-1E**, and **MSNPs-4(2)-1E**, respectively, and the cell viability data as well as fluorescence microscopy images were then obtained. The cell viability (Figure 6a) involving these functional MSNPs at concentrations of 41.7 μg mL^{-1} and 20.8 μg mL^{-1} exhibited a proportional rela-

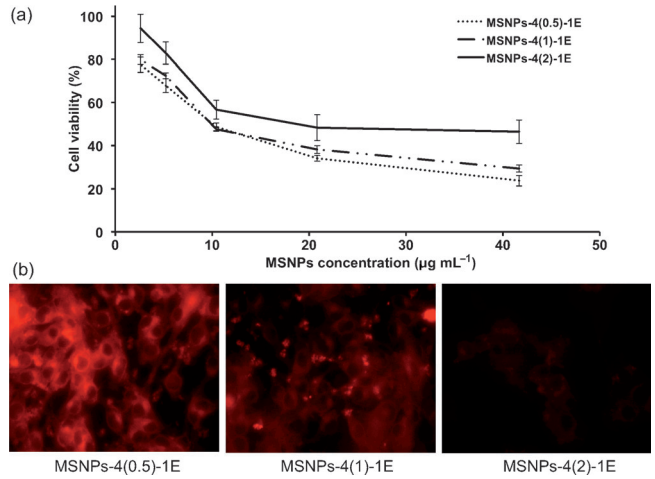

Figure 6. a) Percentage cell viability of B16-F10 after incubation with **MSNPs-4(0.5)-1E**, **MSNPs-4(1)-1E**, and **MSNPs-4(2)-1E** for 4 h before changing the culture media. b) Fluorescence microscopy images of the B16-F10 cell line after incubation with **MSNPs-4(0.5)-1E**, **MSNPs-4(1)-1E**, and **MSNPs-4(2)-1E**.

tionship with the corresponding release profiles (Figure 5). This trend is reasonable because a higher level of drug released would translate to higher cell death, thus causing lower cell viability. At concentrations lower than 20.8 $\mu g\,mL^{-1}$, the difference between the three types of functional MSNPs became insignificant. Therefore, we employed the concentration of 20.8 $\mu g\,mL^{-1}$ for in vitro imaging studies. From the fluorescence images shown in Figure 6b, it was observed that **MSNPs-4(0.5)-1E** gave the strongest red fluorescence intensity compared to the other two samples. This red fluorescence is attributed to DOX, and the intensity observed is proportional to the amount of DOX released into the cells. Hence, it could be concluded that **MSNPs-4(0.5)-1E** showed the highest level of DOX release followed by **MSNPs-4(1)-1E** and lastly **MSNPs-4(2)-1E**. This observation once again supports the results obtained from the cell viability assay as well as the release profile studies.

In conclusion, this work has adopted a supramolecular approach in analyzing the effects of the nature of functional groups on the surface of MSNPs on drug-loading capacity and release kinetics. A catalysis screening method has been employed by first varying chain length, then terminal group, and lastly the amount of thiol units on the surface. The ligand with an intermediate length (5 carbon atoms) and a bulky terminal group (cyclohexyl) shows the highest drug loading and release capacity under the same conditions. To achieve a high drug-release capability, the surface coverage of the ligands should be relatively low. This observation has been further supported by in vitro studies, proving the applicability of the screening method. Guided by the results obtained from this work, better drug delivery systems may be designed for more efficient cancer treatment.

Acknowledgements

This research is supported by the National Research Foundation (NRF), Prime Minister's Office, Singapore under its NRF Fellowship (NRF2009NRF-RF001-015) and Campus for Research Excellence and Technological Enterprise (CREATE) programme—Singapore Peking University Research Centre for a Sustainable Low-Carbon Future, and the NTU-A*Star Centre of Excellence for Silicon Technologies (A*Star SERC No.: 112 351 0003).

Keywords: drug delivery · ligand effects · mesoporous silica nanoparticles · release kinetics · surface functionalization

[1] a) D. Tarn, C. E. Ashley, M. Xue, E. C. Carnes, J. I. Zink, C. J. Brinker, *Acc. Chem. Res.* **2013**, *46*, 792–801; b) M. W. Ambrogio, C. R. Thomas, Y.-L. Zhao, J. I. Zink, J. F. Stoddart, *Acc. Chem. Res.* **2011**, *44*, 903–913; c) M. Vallet-Regí, F. Balas, D. Arcos, *Angew. Chem.* **2007**, *119*, 7692–7703; *Angew. Chem. Int. Ed.* **2007**, *46*, 7548–7558; d) J. L. Vivero-Escoto, I. I. Slowing, B. G. Trewyn, V. S. Y. Lin, *Small* **2010**, *6*, 1952–1967; e) Z. Li, J. C. Barnes, A. Bosoy, J. F. Stoddart, J. I. Zink, *Chem. Soc. Rev.* **2012**, *41*, 2590–2605.

[2] a) N. K. Mal, M. Fujiwara, Y. Tanaka, *Nature* **2003**, *421*, 350–353; b) C. Wang, Z. Li, D. Cao, Y.-L. Zhao, J. W. Gaines, O. A. Bozdemir, M. W. Ambrogio, M. Frasconi, Y. Y. Botros, J. I. Zink, J. F. Stoddart, *Angew. Chem.* **2012**, *124*, 5556–5561; *Angew. Chem. Int. Ed.* **2012**, *51*, 5460–5465; c) Z. Li, J. L. Nyalosaso, A. A. Hwang, D. P. Ferris, S. Yang, G. Derrien, C. Charnay, J.-O. Durand, J. I. Zink, *J. Phys. Chem. C* **2011**, *115*, 19496–19506; d) A. Bernardos, L. Mondragon, E. Aznar, M. D. Marcos, R. Martinez-Manez, F. Sancenon, J. Soto, J. M. Barat, E. Perez-Paya, C. Guillem, P. Amoros, *ACS Nano* **2010**, *4*, 6353–6368.

[3] a) I. Slowing, B. G. Trewyn, V. S. Y. Lin, *J. Am. Chem. Soc.* **2006**, *128*, 14792–14793; b) A. Nieto, M. Colilla, F. Balas, M. Vallet-Regi, *Langmuir* **2010**, *26*, 5038–5049; c) J. C. Doadrio, E. M. B. Sousa, I. Izquierdo-Barba, A. L. Doadrio, J. Perez-Pariente, M. Vallet-Regi, *J. Mater. Chem.* **2006**, *16*, 462–466.

[4] a) E. Aznar, L. Mondragón, J. V. Ros-Lis, F. Sancenón, M. D. Marcos, R. Martínez-Máñez, J. Soto, E. Pérez-Páya, P. Amorós, *Angew. Chem.* **2011**, *123*, 11368–11371; *Angew. Chem. Int. Ed.* **2011**, *50*, 11172–11175; b) Z. Luo, K. Cai, Y. Hu, B. Zhang, D. Xu, *Adv. Healthcare Mater.* **2012**, *1*, 321–325; c) Y.-L. Zhao, Z. Li, S. Kabehie, Y. Y. Botros, J. F. Stoddart, J. I. Zink, *J. Am. Chem. Soc.* **2010**, *132*, 13016–13025; d) C. R. Thomas, D. P. Ferris, J.-H. Lee, E. Choi, M. H. Cho, E. S. Kim, J. F. Stoddart, J.-S. Shin, J. Cheon, J. I. Zink, *J. Am. Chem. Soc.* **2010**, *132*, 10623–10625; e) K. Patel, S. Angelos, W. R. Dichtel, A. Coskun, Y.-W. Yang, J. I. Zink, J. F. Stoddart, *J. Am. Chem. Soc.* **2008**, *130*, 2382–2383; f) H. Yan, C. Teh, S. Sreejith, L. Zhu, A. Kwok, W. Fang, X. Ma, K. T. Nguyen, V. Korzh, Y. Zhao, *Angew. Chem.* **2012**, *124*, 8498–8502; *Angew. Chem. Int. Ed.* **2012**, *51*, 8373–8377; g) C. Park, K. Lee, C. Kim, *Angew. Chem.* **2009**, *121*, 1301–1304; *Angew. Chem. Int. Ed.* **2009**, *48*, 1275–1278; h) C. Y. Ang, S. Y. Tan, X. Wang, Q. Zhang, M. Khan, L. Bai, S. T. Selvan, X. Ma, L. Zhu, K. T. Nguyen, N. S. Tan, Y. Zhao, *J. Mater. Chem. B* **2014**, *2*, 1879–1890.

[5] a) J. Lai, B. P. Shah, E. Garfunkel, K.-B. Lee, *ACS Nano* **2013**, *7*, 2741–2750; b) B. A. Kellogg, L. Garrett, Y. Kovtun, K. C. Lai, B. Leece, M. Miller, G. Payne, R. Steeves, K. R. Whiteman, W. Widdison, H. Xie, R. Singh, R. V. J. Chari, J. M. Lambert, R. J. Lutz, *Bioconjugate Chem.* **2011**, *22*, 717–727; c) P. E. Thorpe, P. M. Wallace, P. P. Knowles, M. G. Relf, A. N. F. Brown, G. J. Watson, D. C. Blakey, D. R. Newell, *Cancer Res.* **1988**, *48*, 6396–6403; d) A. N. Koo, H. P. Rim, D. J. Park, J.-H. Kim, S. Y. Jeong, S. C. Lee, *Macromol. Res.* **2013**, *21*, 809–814.

[6] a) J. A. Cook, H. I. Pass, S. N. Iype, N. Friedman, W. Degraff, A. Russo, J. B. Mitchell, *Cancer Res.* **1991**, *51*, 4287–4294; b) M. J. Allalunisturner, F. Y. F. Lee, D. W. Siemann, *Cancer Res.* **1988**, *48*, 3657–3660.

[7] a) X. Ma, K. T. Nguyen, P. Borah, C. Y. Ang, Y. Zhao, *Adv. Healthcare Mater.* **2012**, *1*, 690–697; b) Y. Cui, H. Dong, X. Cai, D. Wang, Y. Li, *ACS Appl. Mater. Interfaces* **2012**, *4*, 3177–3183; c) Z. Luo, K. Cai, Y. Hu, L. Zhao, P. Liu, L. Duan, W. Yang, *Angew. Chem.* **2011**, *123*, 666–669; *Angew. Chem. Int. Ed.* **2011**, *50*, 640–643; d) Q. Zhang, F. Liu, K. T. Nguyen, X. Ma, X.

Wang, B. Xing, Y. Zhao, *Adv. Funct. Mater.* **2012**, *22*, 5144 – 5156; e) H. Kim, S. Kim, C. Park, H. Lee, H. J. Park, C. Kim, *Adv. Mater.* **2010**, *22*, 4280 – 4283.

[8] L. Du, S. Liao, H. A. Khatib, J. F. Stoddart, J. I. Zink, *J. Am. Chem. Soc.* **2009**, *131*, 15136 – 15142.

[9] E. Aznar, F. Sancenón, M. D. Marcos, R. Martínez-Máñez, P. Stroeve, J. Cano, P. Amorós, *Langmuir* **2012**, *28*, 2986 – 2996.

[10] P. Nadrah, U. Maver, A. Jemec, T. Tisler, M. Bele, G. Drazic, M. Bencina, A. Pintar, O. Planinsek, M. Gaberscek, *ACS Appl. Mater. Interfaces* **2013**, *5*, 3908 – 3915.

[11] a) Z. Luo, X. Ding, Y. Hu, S. Wu, Y. Xiang, Y. Zeng, B. Zhang, H. Yan, H. Zhang, L. Zhu, J. Liu, J. Li, K. Cai, Y. Zhao, *ACS Nano* **2013**, *7*, 10271 – 10284; b) Q. Zhang, X. Wang, P.-Z. Li, K. T. Nguyen, X.-J. Wang, Z. Luo, H. Zhang, N. S. Tan, Y. Zhao, *Adv. Funct. Mater.* **2014**, *24*, 2450 – 2461.

Received: May 16, 2014
Published online on ■■ ■■, 0000

COMMUNICATION

Drug Delivery

*S. Y. Tan, C. Y. Ang, P. Li, Q. M. Yap, Y. Zhao**

■■ – ■■

Drug Encapsulation and Release by Mesoporous Silica Nanoparticles: The Effect of Surface Functional Groups

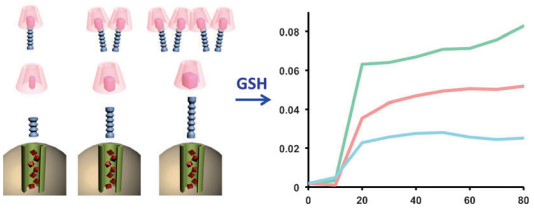

Maximizing drug release from drug carriers is important to achieve better therapeutic efficiency. Using glutathione (GSH)-triggered drug-release systems as a case study, the effect of the nature of surface functional groups on mesoporous silica nanoparticles on drug-loading and drug-release capabilities was investigated.

Controlled Drug Delivery

Maximizing drug release from drug carriers is important to achieve better therapeutic efficiency. In their Communication on page ■■ ff., Y. Zhao et al. show how a catalysis screening technique can be adopted for analyzing the effects of chain length, terminal group, and density of functional ligands on the surface of mesoporous silica nanoparticles on drug-loading capacity and glutathione-triggered drug-release kinetics. The results obtained may serve as a general guide for developing more effective carriers for drug delivery.